The Effect of a Modulated Cellular Detonation Structure on the Wave Transmission across an Inert Layer

Kelsey C. Tang-Yuk[a], John H.S. Lee[a], Georgios Bakalis[b], Hoi Dick Ng[b], Xiaocheng Mi[c]

[a]Department of Mechanical Engineering, McGill University, Montreal, QC, Canada.
[b]Department of Mechanical, Industrial, and Aerospace Engineering, Concordia University, Montreal, QC, Canada.
[c]Eindhoven Institute of Renewable Energy Systems, Eindhoven University of Technology, Eindhoven, the Netherlands.

1 Introduction

Gaseous detonation waves are inherently unstable, with a cellular frontal structure that is characteristic of the reactive mixture. Recently, a method has been proposed to modulate this inherent transverse wave structure of the detonation wave by embedding micro-plates in the reactive gas as shown in figure 1(a). Through this methodology, the detonation structure can be altered without affecting the detonation velocity, see [2].

In addition, a simple transmission problem has been explored in previous work [3, 4], namely the transmission of the detonation wave across a layer, or pocket, of inert gas as shown in figure 1(b). The detonation wave is progressively damped as it transmits across the inert layer, and so detonation re-initiation downstream of the inert layer depends on the thickness of the layer. A critical inert layer thickness, $\delta_{\mathrm{i,cr}}$, beyond which the detonation cannot be re-initiated in the downstream reactive region, can be identified.

In the present work, the goal is to explore the effect of altering the cellular structure on the detonation dynamics in critical phenomena. To this end, the effect of a modulated cellular structure (obtained by a specific arrangement of these micro-plates) on the inert layer problem is investigated via numerical simulation.

2 Simulation details

The governing equations are the two-dimensional reactive Euler equations, coupled with the two-step induction-reaction kinetics model [5]. The induction length of the corresponding steady Zel'dovich-von Neumann-Döring (ZND) detonation, Δ_{I}, is set to unity. The chemical kinetic model, non-dimensionalization of state and flow variables, and the scaling of rate constants are detailed in [5].

The reactive gas mixture was selected to be one which gives an irregular cellular pattern, and to be consistent with previous work [4] for ease of comparison. Specifically, the non-dimensional parameters are set to $\gamma = 1.2$, $Q = 50$, $E_{\mathrm{i}} = 9T_{\mathrm{vn}}$, $E_{\mathrm{r}} = T_{\mathrm{vn}}$, $k_{\mathrm{i}} = 0.7792$, and $k_{\mathrm{r}} = 0.8$. In addition, a

Correspondence to: kelsey.tangyuk@mail.mcgill.ca

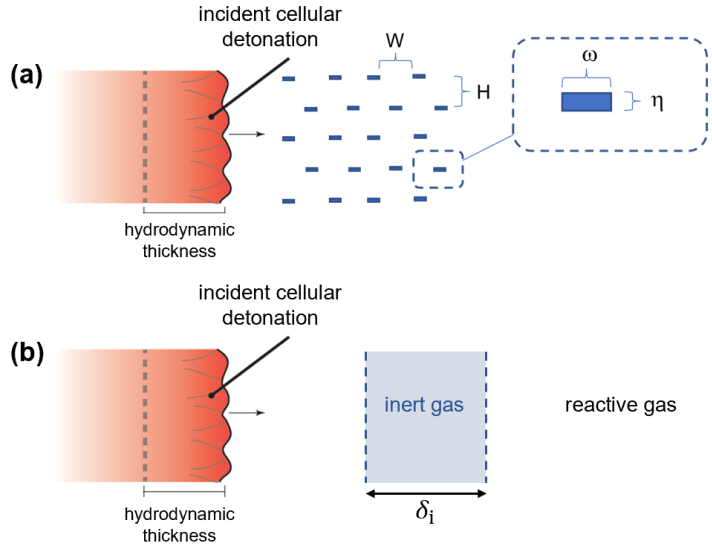

Figure 1: Schematic illustration showing: **(a)** micro-plates embedded in the detonable gas in order to modulate the detonation structure, and **(b)** the transmission of a detonation wave across a layer of inert gas.

specific arrangement of the micro-plates was chosen, with $W = 25$, $H = 10$, $\omega = 15$ and $\eta = 0.5$ (see figure 1(a)).

The simulation was based upon a uniform Cartesian grid, with a grid resolution of 10 grid points per Δ_I. The MUSCL-Hancock scheme with the van Leer non-smooth slope limiter and a Harten-Lax-van Leer-contact (HLLC) approximate solver was used [6]. A periodic boundary condition was applied to the top and bottom of the domain, with reflective boundary conditions for the obstacles, and transmissive left and right boundaries.

3 Statistical methodology

3.1 Average shock pressure

The two-dimensional flowfield was first spatially averaged to obtain a one-dimensional flowfield by averaging across the vertical y-axis. The average shock location, x_{shock}, was defined to be where the average pressure becomes greater than some threshold pressure, and its location was calculated by interpolation. When repeated throughout the decay, x_{shock} was obtained as a function of time, and the average shock speed M_{shock} can be calculated. Finally, the average shock pressure p_{shock} was found from M_{shock} with the Rankine-Hugoniot relations.

3.2 One-dimensional average profile

The spatially averaged data above may now also be temporally averaged. The flowfield data were transformed to a wave-attached reference frame, which in this case is a frame moving at the Chapman-Jouguet (CJ) speed. Where the bar accent ($\bar{}$) represents these spatially and temporally averaged values, the average reaction rate is given by,

$$\bar{\Omega} = \bar{\rho} k_r (1 - \bar{\lambda_0}) \exp\left(\frac{E_r}{\bar{T}}\right). \tag{1}$$

More details on the calculation of this type of average profile can be found in [7]. The profiles were calculated over a wave propagation distance of at least $1000\Delta_{\mathrm{I}}$, which contains ~ 2000 flowfield excerpts.

3.3 Maximum pressure statistical analysis

A novel method of characterizing the strength of the detonation front cellular structure is proposed. The maximum pressure, $p_{\max}$, obtained at each computational grid point is recorded in the numerical soot foils. These data are used to calculate a probability density function (PDF) over this variable $p_{\max}$. For a steady-state detonation, the PDF shows the distribution of shock pressures at the detonation front. For transient processes such as the wave transmission into the inert layer, a similar analysis can be performed. In this case the distribution is no longer spatially independent and the idea is to find multiple PDFs of $p_{\max}$ (as before), one at each x-location throughout the process. Therefore, the PDF shows how the shock pressure distribution changes.

The range of $p_{\max}$ considered, i.e., the minimum and maximum values are 20 and 80, respectively. This ranges from approximately half to twice the von Neumann shock pressure ($p_{\mathrm{vn}} \approx 42$) in order to capture the majority of shock pressure values. The steady-state statistics are gathered over a wave propagation distance of at least $2000\Delta_{\mathrm{I}}$, which contains least 6e7 data points. In the transient case the statistics are gathered over 8 runs, where for each run the incident detonation is varied. This gives $\sim$ 3e5 data points for each PDF (at each x-location).

4 Results and discussion

4.1 The modulated detonation structure

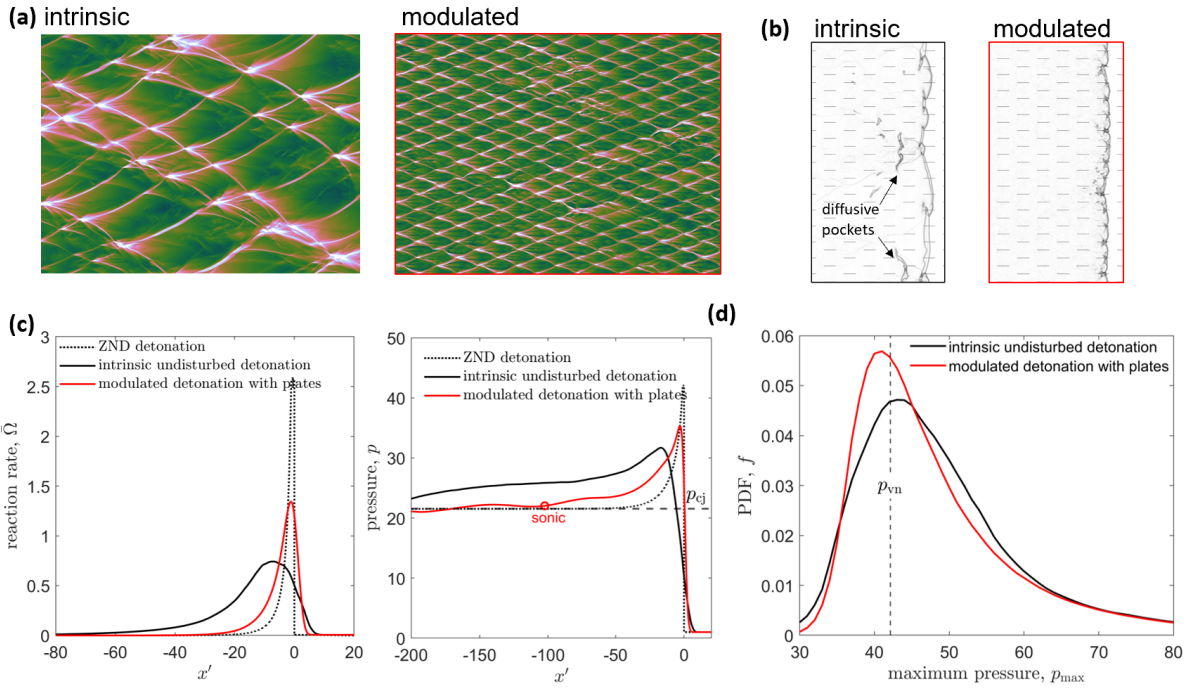

Figure 2: **(a)**Numerical soot foils, **(b)** schlieren images of the flowfield, **(c)** the average one-dimensional reaction rate, $\bar{\Omega}$, and pressure, $\bar{p}$, profiles compared to the ZND, and **(d)** the probability density functions (PDFs), f, of the maximum pressure, $p_{\max}$, for the intrinsic undisturbed and modulated detonations.

In figure 2, the undisturbed intrinsic detonation and the modulated detonation obtained with the chosen arrangement of micro-plates are compared. Note that because the plates are very thin ($\eta = 0.5$), there is no velocity deficit in the propagation direction and so both waves propagate on average at the CJ velocity. Therefore, a direct comparison can be made between the two wave structures.

Figures 2(a) and (b) show numerical soot foils and schlieren images of the flowfield, respectively. In the soot foils of figure 2(a), the inherent detonation cellular structure can be seen to be highly irregular with non-uniform cell size, while the modulation produces highly regular cells. A typical feature of unstable detonations with irregular cells is the presence of pockets of gas that do not burn by shock compression only, but via slower diffusive processes further downstream [8]. These pockets are seen in the original detonation structure of figure 2(b), but are notably absent in the modulated structure. Thus, for the modulated detonation the reactive mixture burns relatively uniformly by shock compression, as is typical for detonations which exhibit regular cellular structures [8].

In figure 2(c), the average one-dimensional reaction rate and pressure profiles are plotted, along with the ZND structure. The reaction zone thickness of the intrinsic detonation is much larger than that of the ZND wave. The modulated wave more closely approaches the ZND structure with a thinner reaction zone. The approach of the products to the CJ equilibrium pressure corresponds to the location of the sonic plane which defines the hydrodynamic thickness [9]. From the intrinsic to the modulated structure, the hydrodynamic thickness has similarly been reduced to more closely approach the ZND structure.

Finally, the PDFs of maximum pressure are plotted in figure 2(d). Recall that the PDFs show the distribution of shock pressures at the detonation front. Both PDFs peak near p_{vn}, however, the intrinsic structure shows a larger pressure range with greater occurrence of high-pressure values (above $\sim p = 45$). Therefore, the shock structure of the modulated detonation is less fluctuating, which is again more similar to that of the non-fluctuating ZND leading shock.

4.2 The critical phenomenon

First, consider the transmission of the detonation wave from the reactive to inert gas only. This will describe the transmitted wave at the exit of the inert layer for any given inert thickness, δ_{i}. In figure 3, the transient process is compared for incident intrinsic and modulated detonations, as well as for the case of an incident 1D ZND detonation. Figures 3(a) and (b) show numerical soot foils and PDFs of the maximum pressure for the two incident cellular detonations. In figure 3(c) the change in 2D average shock pressure in the cellular cases, or 1D shock pressure in the ZND case, is plotted. The interface between reactive to inert gas lies at $x = 0$ as indicated by the vertical dashed line on all plots.

For the incident detonations, p_{shock} is always at (or fluctuates around) p_{vn}. After the detonation enters the inert gas, p_{shock} decreases, the PDF shock pressure range narrows, and the cellular structure disappears from the soot foils. Eventually, a final planar shock with pressure, p_{f} is obtained. For the incident intrinsic detonation, the PDF indicates that portions of the leading shock exceed p_{vn} until about $x_{\mathrm{shock}} = 150$, which corresponds roughly to the disappearance of the cellular structure in the soot foil. Therefore, after this point there has been significant damping of the transverse waves. In addition, the full relaxation of p_{shock} to p_{f} is realized by about $x_{\mathrm{shock}} = 700$. For the modulated detonation the relaxation process is significantly shorter, with shock pressures above p_{vn} disappearing by about $x_{\mathrm{shock}} = 50$, and full relaxation being achieved around $x_{\mathrm{shock}} = 150$. Finally, notice that the decay in average shock pressure for this modulated detonation case matches that for the ZND detonation.

Now consider a layer of inert gas with finite thickness, δ_{i}. Typical numerical soot foils for the incident modulated detonation are shown in figure 4, where the inert layer thicknesses are $\delta_{\mathrm{i}} = 25$ and 50, respectively. The vertical dashed lines show the two boundaries of the inert layer. When $\delta_{\mathrm{i}} \leq 25$, the

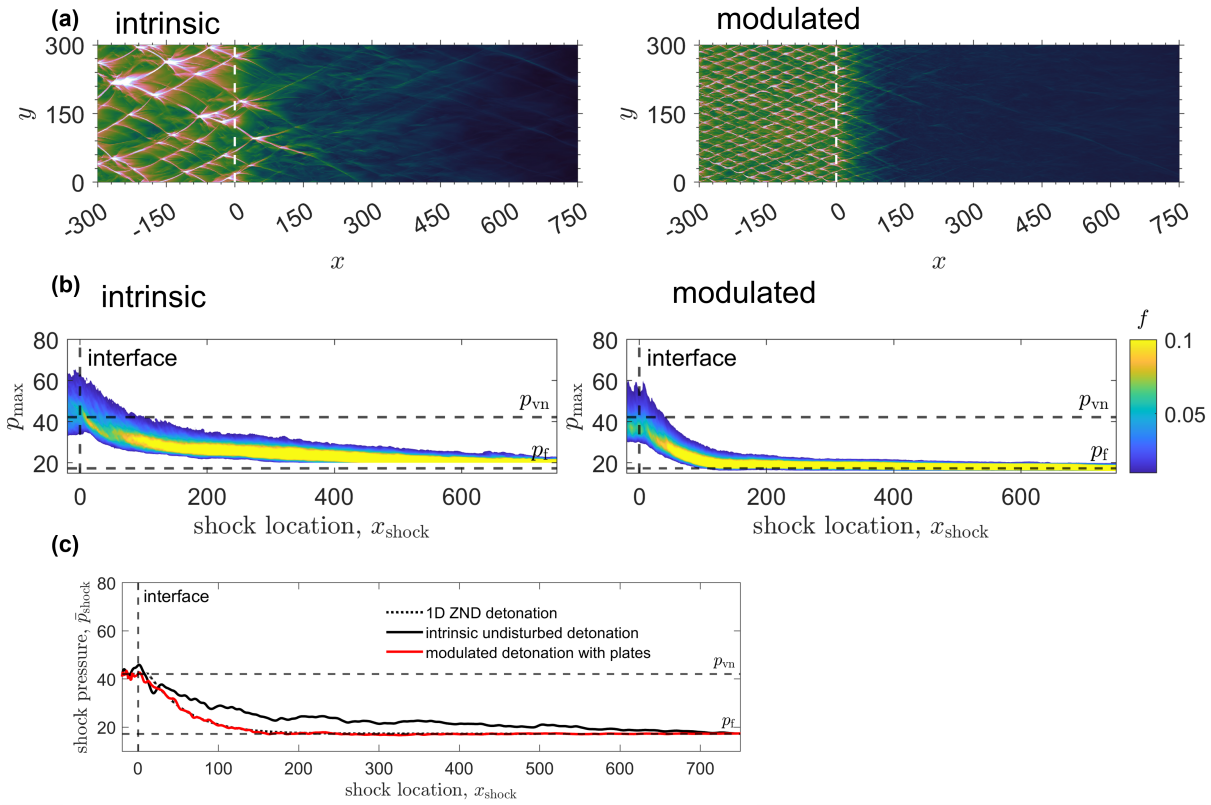

Figure 3: The detonation transmission from reactive to inert gas for the incident intrinsic undisturbed detonation and the incident modulated detonation with micro-plates via: **(a)** numerical soot foils, **(b)** the probability density functions (PDFs) of the maximum pressure, and **(c)** the average shock pressure compared to that for a one-dimensional incident ZND wave. The vertical dashed line at $x = 0$ indicates the boundary between the reactive and inert gases.

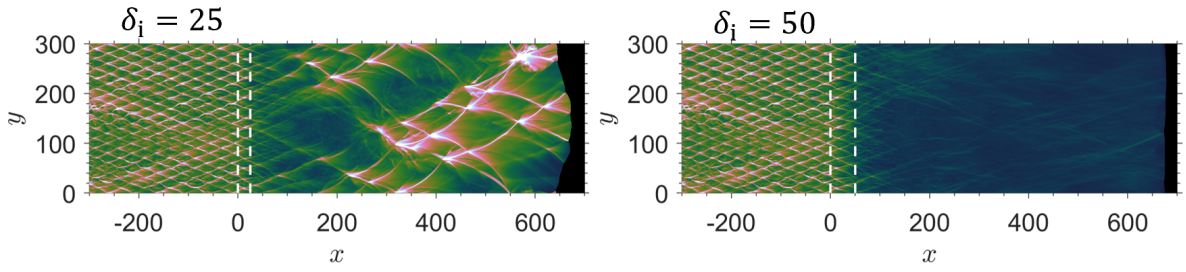

Figure 4: Numerical soot foils for the transmission of the incident modulated detonation across inert layers with thicknesses $\delta_i = 25$ and 50. The vertical dashed lines indicate the initial upstream and downstream boundaries of the inert layer.

detonation is successfully transmitted downstream of the inert layer, but when $\delta_i \geq 50$, the detonation cannot be re-initiated downstream. Therefore, the critical thickness, $\delta_{i,cr}$ is 37.5 ± 12.5.

In previous studies [3, 4], the critical inert thicknesses for the intrinsic undisturbed detonation and the 1D ZND detonation were estimated. These values are tabulated in table 1. Again, the critical thickness for the modulated detonation is closer to that for the ZND case. However, the critical thicknesses for both cellular detonations are still larger than in the ZND case. In a previous study [4], re-initiation was attributed to the residual cellular structure of the transmitted shock at the exit of the inert layer. It is inter-

esting to note that, in agreement with this, the critical condition for both cellular cases corresponds with the disappearance of portions of the wave with shock strengths above p_{vn} and of the cellular structure on the soot foils as was seen in figures 3(a) and (b).

Table 1: Critical inert thicknesses for incident ZND, intrinsic undisturbed, and modulated detonations.

Incident detonation	**Critical thickness,** $\delta_{\mathrm{i,cr}}$
1D ZND detonation	3
intrinsic undisturbed detonation	170
modulated detonation with plates	37.5

5 Concluding remarks

The intrinsic detonation structure was modulated by the inclusion of micro-plates, and the effect of this modulation on a critical phenomenon was investigated, namely the wave transmission across an inert layer. The structure of the modulated detonation is closer to the one-dimensional ZND structure in that it was found to have a thinner reaction zone with reactions dominated by shock ignition, and a smaller hydrodynamic thickness. Therefore, the modulated detonation was found to be more congruent with the ZND solution in aspects of the critical phenomenon, specifically the relaxation in the inert gas and the critical inert thickness. More generally, the present results suggest that the detonation structure can be modulated so that its dynamic parameters may be better controlled and moreover predicted by one-dimensional theory. A resolution study is currently underway.

References

[1] J.H.S. Lee. (2008). The Detonation Phenomenon. Cambridge University Press.

[2] K.C. Tang-Yuk, G. Bakalis, H.D. Ng, X. Mi, An Approach to Modulate the Frontal Detonation structures in Numerical Simulations, 29th ICDERS, (2023).

[3] K.C. Tang-Yuk, X. Mi, J.H. Lee, H.D. Ng, and R. Deiterding, Transmission of a detonation wave across an inert layer, Combust. Flame, 236 (2022), 111769.

[4] K.C. Tang-Yuk, J.H. Lee, H.D. Ng, R. Deiterding, and X. Mi (in press), The re-initiation of cellular detonations downstream of an inert layer. Proc. Combust. Inst. (2022).

[5] H.D. Ng, M.I. Radulescu, A.J. Higgins, N. Nikiforakis, J.H. Lee, Numerical investigation of the instability for one-dimensional Chapman-Jouguet detonations with chain-branching kinetics, Combust. Theor. Model 9 (2005) 385–401.

[6] E.F. Toro, Riemann Solvers and Numerical Methods for Fluid Dynamics, Springer-Verlag, 1997.

[7] X.C. Mi, A.J. Higgins, H.D. Ng, C.B. Kiyanda, and N. Nikiforakis, Propagation of gaseous detonation waves in a spatially inhomogeneous reactive medium, Phys. Rev. Fluids, 2(5) (2017) 053201.

[8] M.I. Radulescu, H.D. Ng, J.H. Lee, and B. Varatharajan, The effect of argon dilution on the stability of acetylene/oxygen detonations, Proc. Combust. Inst., 29(2) (2002) 2825–2831.

[9] J.H.S, Lee, and M.I. Radulescu, On the hydrodynamic thickness of cellular detonations, Combustion, Explosion and Shock Waves, 41(6) (2005) 745–765.